

---

# Deep RBF Value Functions for Continuous Control

---

Kavosh Asadi<sup>1</sup> Ronald E. Parr<sup>2</sup> George D. Konidaris<sup>1</sup> Michael L. Littman<sup>1</sup>

## Abstract

A core operation in reinforcement learning (RL) is finding an action that is optimal with respect to a learned state–action value function. This operation is often challenging when the learned value function takes continuous actions as input. We introduce deep RBF value functions: state–action value functions learned using a deep neural network with a radial-basis function (RBF) output layer. We show that the optimal action with respect to a deep RBF value function can be easily approximated up to any desired accuracy. Moreover, deep RBF value functions can represent any true value function up to any desired accuracy owing to their support for universal function approximation. By learning a deep RBF value function, we extend the standard DQN algorithm to continuous control, and demonstrate that the resultant agent, RBF–DQN, outperforms standard baselines on a set of continuous-action RL problems.

## 1. Introduction

A fundamental quantity of interest in RL is the state–action value ( $Q$ ) function, which quantifies the expected return for taking action  $a$  in state  $s$ . Many RL algorithms, notably Q-learning (Watkins, 1989), learn an approximation of the  $Q$  function from environmental interactions. When using function approximation with Q-learning, the agent has a parameterized function class, and learning consists of finding a parameter setting  $\theta$  for the approximate value function  $\widehat{Q}(s, a; \theta)$  that accurately represents the true  $Q$  function. A core operation here is finding an optimal action with respect to the value function,  $\arg \max_a \widehat{Q}(s, a; \theta)$ , or finding the highest action-value  $\max_a \widehat{Q}(s, a; \theta)$ . The need for performing these operations arises not just when computing a behavior policy for action selection, but also when learning  $Q$  itself using bootstrapping techniques

(Sutton & Barto, 2018).

The optimization problem  $\max_{a \in \mathcal{A}} \widehat{Q}(s, a; \theta)$  is generally challenging if  $\mathcal{A}$  is continuous, in contrast to the discrete case where the operation is trivial if the number of discrete actions is not enormous. The challenge stems from the observation that the surface of the function  $f_s(a; \theta) := \widehat{Q}(s, a; \theta)$  could have many local maxima and saddle points; therefore, naïve approaches such as finding the maximum through gradient ascent can lead into inaccurate answers (Ryu et al., 2019). In light of this technical challenge, recent work on solving continuous control problems has instead embraced policy-gradient algorithms, which typically compute  $\nabla_a \widehat{Q}(s, a; \theta)$ , rather than solving  $\max_{a \in \mathcal{A}} \widehat{Q}(s, a; \theta)$ , and follow the ascent direction to move an explicitly maintained policy towards actions with higher  $\widehat{Q}$  (Silver et al., 2014). However, policy-gradient algorithms have their own weaknesses, particularly in settings with sparse rewards where computing an accurate estimate of the gradient requires an unreasonable number of environmental interactions (Kakade & Langford, 2002; Matheron et al., 2019). Rather than adopting a policy-gradient approach, we focus on tackling the problem of efficiently computing  $\max_{a \in \mathcal{A}} \widehat{Q}(s, a; \theta)$  for value-function-based RL.

Previous work on value-function-based algorithms for continuous control has shown the benefits of using function classes that are conducive to efficient action maximization. For example, Gu et al. (2016) explored function classes that can capture an arbitrary dependence on the state, but only a quadratic dependence on the action. Given a function class with a quadratic dependence on the action, Gu et al. (2016) showed how to compute  $\max_{a \in \mathcal{A}} \widehat{Q}(s, a; \theta)$  quickly and in constant time. A more general idea is to use input–convex neural networks (Amos et al., 2017) that restrict  $\widehat{Q}(s, a; \theta)$  to functions that are convex (or concave) with respect to  $a$ , so that for any fixed state  $s$  the optimization problem  $\max_{a \in \mathcal{A}} \widehat{Q}(s, a; \theta)$  can be solved efficiently using convex-optimization techniques (Boyd & Vandenberghe, 2004). These solutions trade the expressiveness of the function class for easy action maximization.

While restricting the function class can enable easy maximization, it can be problematic if no member of the restricted class has low approximation error relative to the

<sup>1</sup>Department of Computer Science, Brown University.  
<sup>2</sup>Department of Computer Science, Duke University.  
Correspondence to: Kavosh Asadi <kavosh@brown.edu>.

true  $Q$  function (Lim et al., 2018). More concretely, when the agent cannot possibly learn an accurate  $\widehat{Q}$ , the error  $|\max_a Q^\pi(s, a) - \max_a \widehat{Q}(s, a; \theta)|$  could be significant even if the agent can solve  $\max_a \widehat{Q}(s, a; \theta)$  exactly. In the case of input-convex neural networks, for example, high error can occur if  $f_a(s; \theta) := \widehat{Q}(s, a; \theta)$  is completely non-convex. Thus, it is desirable to ensure that, for any true  $Q$  function, there exists a member of the function class that approximates  $Q$  up to any desired accuracy. Such a function class is said to be capable of universal function approximation (UFA) (Hornik et al., 1989; Benaim, 1994; Hammer & Gersmann, 2003). A function class that is both conducive to efficient action maximization and also capable of UFA would be ideal.

We introduce deep RBF value functions, which approximate  $Q$  by a standard deep neural network equipped with an RBF output layer. We show that deep RBF value functions have the two desired properties outlined above: First, using deep RBF value functions enable us to approximate the optimal action up to any desired accuracy. Second, deep RBF value functions support universal function approximation.

Prior work in RL used RBF networks for learning the state-value function ( $V$ ) in problems with discrete action spaces (see Section 9.5.5 of Sutton & Barto (2018) for a discussion). That said, to the best of our knowledge, our discovery of the action-maximization property of RBF networks is novel, and there has been no application of deep RBF networks to continuous control. We combine deep RBF networks with DQN (Mnih et al., 2015), a standard deep RL algorithm originally proposed for discrete actions, to produce a new algorithm called RBF-DQN. We evaluate RBF-DQN on a large set of continuous-action RL problems, and demonstrate its superior performance relative to standard deep-RL baselines.

## 2. Background

We study the interaction between an environment and an agent that seeks to maximize reward (Sutton & Barto, 2018), a problem typically formulated using Markov Decision Processes (MDPs) (Puterman, 2014). An MDP is usually specified by a tuple:  $\langle \mathcal{S}, \mathcal{A}, T, R, \gamma \rangle$ . In this work,  $\mathcal{S}$  and  $\mathcal{A}$  denote the continuous state space and the continuous action space of the MDP. The MDP model is comprised of two functions, namely the transition model  $T : \mathcal{S} \times \mathcal{A} \times \mathcal{S} \rightarrow [0, 1]$ , and the reward model  $R : \mathcal{S} \times \mathcal{A} \rightarrow \mathcal{R}$ . The discount factor,  $\gamma \in [0, 1]$ , determines the importance of immediate reward as opposed to rewards received in the future. The goal of an RL agent is to find a policy,  $\pi : \mathcal{S} \rightarrow \mathcal{A}$  that collects high sums of discounted rewards across timesteps.

For a state  $s \in \mathcal{S}$ , action  $a \in \mathcal{A}$ , and a policy  $\pi$ , we define

the state-action value function:

$$Q^\pi(s, a) := \mathbf{E}_\pi[G_t \mid s_t = s, a_t = a],$$

where  $G_t := \sum_{i=t}^{\infty} \gamma^{i-t} R_i$  is called the *return* at timestep  $t$ . The state-action value function of an *optimal* policy, denoted by  $Q^*(s, a)$ , can be written recursively (Bellman, 1952):

$$Q^*(s, a) = R(s, a) + \gamma \int_{s'} T(s, a, s') \max_{a'} Q^*(s', a') ds'. \quad (1)$$

If the model of the MDP  $\langle R, T \rangle$  is available, standard dynamic programming approaches find  $Q^*$  by solving for the fixed point of (1), known as the Bellman equation.

In the absence of a model, a class of RL algorithms solve for the fixed point of the Bellman equation using environmental interactions and without learning a model. Q-learning (Watkins, 1989), a notable example of these so-called model-free algorithms, learns an approximation of  $Q^*$ , denoted by  $\widehat{Q}$  and parameterized by  $\theta$ . When combined with function approximation, Q-learning updates  $\theta$  parameters as follows:

$$\begin{aligned} \theta &\leftarrow \theta + \alpha \delta \nabla_\theta \widehat{Q}(s, a; \theta), \\ \text{where } \delta &:= r + \gamma \max_{a' \in \mathcal{A}} \widehat{Q}(s', a'; \theta) - \widehat{Q}(s, a; \theta), \end{aligned} \quad (2)$$

using tuples of experience  $\langle s, a, r, s' \rangle$  observed during environmental interactions. The quantity  $\delta$  is often referred to as the temporal difference (TD) error (Sutton, 1988).

Note that Q-learning’s update rule (2) is agnostic to the choice of function class, and so in principle any differentiable and parameterized function class could be used in conjunction with the above update to learn  $\theta$  parameters. For example, Sutton (1996) used linear function approximation, Konidaris et al. (2011) used Fourier basis functions, and Mnih et al. (2015) chose the class of convolutional neural networks and showed remarkable results for learning to play Atari games.

## 3. Deep RBF Value Functions

Deep RBF value functions combine the practical advantages of deep networks (Goodfellow et al., 2016) with the theoretical advantages of radial-basis functions (RBFs) (Powell, 1987). A deep RBF network is comprised of a number of arbitrary hidden layers, followed by an *RBF output layer*, defined next. The RBF output layer, first introduced in a seminal paper by Broomhead & Lowe (1988), is sometimes used as a standalone single-layer function approximator, referred to as a (shallow) RBF network. We use an RBF network as the final, or output, layer of a deep network.

For a given input  $a$ , the RBF layer  $f(a)$  is defined as:

$$f(a) := \sum_{i=1}^N g(a - a_i) v_i, \quad (3)$$

where each  $a_i$  represents a *centroid* location,  $v_i$  is the value of the centroid  $a_i$ ,  $N$  is the number of centroids, and  $g$  is an RBF. A commonly used RBF is the negative exponential:

$$g(a - a_i) := e^{-\beta \|a - a_i\|}, \quad (4)$$

equipped with a smoothing parameter  $\beta \geq 0$ . (See Karayiannis (1999) for a thorough treatment of other RBFs.) Formulation (3) could be thought of as an interpolation based on the value and the weights of all centroids, where the weight of each centroid is determined by its proximity to the input. Proximity here is quantified by the RBF  $g$ , in this case the negative exponential (4).

As will be clear momentarily, it is theoretically useful to normalize centroid weights to ensure that they sum to 1 so that  $f$  implements a weighted average. This weighted average is sometimes referred to as a normalized Gaussian RBF layer (Moody & Darken, 1989; Bugmann, 1998):

$$f_\beta(a) := \frac{\sum_{i=1}^N e^{-\beta \|a - a_i\|} v_i}{\sum_{i=1}^N e^{-\beta \|a - a_i\|}}. \quad (5)$$

As the smoothing parameter  $\beta \rightarrow \infty$  the function implements a winner-take-all case where the value of the function at a given input is determined only by the value of the closest centroid location, nearest-neighbor style. This limiting case is sometimes referred to as a *Voronoi decomposition* (Aurenhammer, 1991). Conversely,  $f$  converges to the mean of centroid values regardless of the input  $a$  as  $\beta$  gets close to 0; that is,  $\forall a \lim_{\beta \rightarrow 0} f_\beta(a) = \frac{\sum_{i=1}^N v_i}{N}$ . Since an RBF layer is differentiable, it could be used in conjunction with (stochastic) gradient descent and backprop to learn the centroid locations and their values by optimizing for a loss function. Note that formulation (5) is different than the Boltzmann softmax operator (Asadi & Littman, 2017; Song et al., 2019), where the weights are determined, not by an RBF, but by the action values.

Finally, to represent the  $Q$  function for RL, we use the following formulation:

$$\hat{Q}_\beta(s, a; \theta) := \frac{\sum_{i=1}^N e^{-\beta \|a - a_i(s; \theta)\|} v_i(s; \theta)}{\sum_{i=1}^N e^{-\beta \|a - a_i(s; \theta)\|}}. \quad (6)$$

A deep RBF  $Q$  function (6) internally learns two mappings: state-dependent set of centroid locations  $a_i(s; \theta)$  and state-dependent centroid values  $v_i(s; \theta)$ . The role of the RBF output layer, then, is to use these learned mappings to form the output of the entire deep RBF  $Q$  function. We

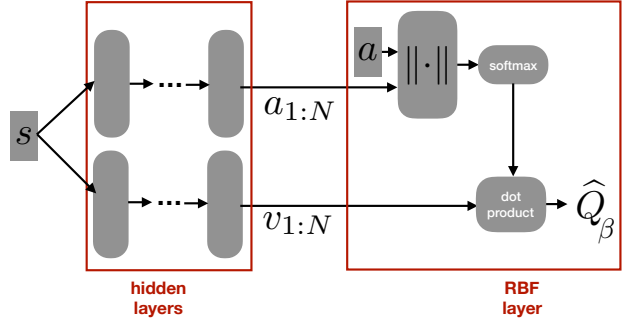


Figure 1. The architecture of a deep RBF value ( $Q$ ) function. A deep RBF  $Q$  function could be thought of as an RBF output layer added to an otherwise standard deep state-action value ( $Q$ ) function. In this sense, any kind of standard layer (dense, convolutional, recurrent, etc.) could be used as a hidden layer. All operations of the final RBF layer are differentiable, and therefore, the parameters of hidden layers  $\theta$ , which represent the mappings  $a_i(s; \theta)$  and  $v_i(s; \theta)$ , can be learned using standard gradient-based optimization techniques.

illustrate the architecture of a deep RBF  $Q$  function in Figure 1. In the experimental section, we demonstrate how to learn parameters  $\theta$ .

We now show that deep RBF function have the first desired property for value-function-based RL, namely that they enable easy action maximization.

In light of the RBF formulation, it is easy to find the value of the deep RBF  $Q$  function at each centroid location  $a_i$ , that is, to compute  $\hat{Q}_\beta(s, a_i; \theta)$ . Note that  $\hat{Q}_\beta(s, a_i; \theta) \neq v_i(s; \theta)$  in general for a finite  $\beta$ , because the other centroids  $a_j \forall j \in \{1, \dots, N\} - i$  may have non-zero weights at  $a_i$ . In other words, the action-value function at a centroid  $a_i$  can in general differ from the centroid's value  $v_i$ .

Therefore, to compute  $\hat{Q}_\beta(s, a_i; \theta)$ , we access the centroid location using  $a_i(s; \theta)$ , then input  $a_i$  to get  $\hat{Q}(s, a_i; \theta)$ . Once we have  $\hat{Q}(s, a_i; \theta) \forall a_i$ , we can trivially find the highest-valued centroid or its corresponding  $\hat{Q}$ :

$$\max_{i \in [1, N]} \hat{Q}_\beta(s, a_i; \theta).$$

While in general there may be a gap between the global maximum  $\max_{a \in \mathcal{A}} \hat{Q}_\beta(s, a; \theta)$  and its easy-to-compute approximation  $\max_{i \in [1, N]} \hat{Q}_\beta(s, a_i; \theta)$ , the following theorem predicts that this gap is zero in one-dimensional action spaces. More importantly, Theorem 1 guarantees that in action spaces with an arbitrary number of dimensions, the gap gets exponentially small with increasing the smoothing parameter  $\beta$ , allowing us to reduce the gap very quickly and up to any desired accuracy by simply increasing the smoothing parameter  $\beta$ .

**Theorem 1.** Let  $\widehat{Q}_\beta$  be a member of the class of normalized Gaussian RBF value functions.

I) For a one-dimensional action space  $\mathcal{A} = \mathcal{R}$ :

$$\max_{a \in \mathcal{A}} \widehat{Q}_\beta(s, a; \theta) = \max_{i \in [1, N]} \widehat{Q}_\beta(s, a_i; \theta).$$

II) For  $\mathcal{A} = \mathcal{R}^d \quad \forall d \geq 1$ :

$$0 \leq \max_{a \in \mathcal{A}} \widehat{Q}_\beta(s, a; \theta) - \max_{i \in [1, N]} \widehat{Q}_\beta(s, a_i; \theta) \leq \mathcal{O}(e^{-\beta}).$$

*Proof.* See Appendix.  $\square$

Figure 2 shows an example of the output of an RBF  $Q$  function where there exists a gap between  $\max_{a \in \mathcal{A}} \widehat{Q}_\beta(s, a; \theta)$  and  $\max_{i \in [1, N]} \widehat{Q}_\beta(s, a_i; \theta)$  for small values of  $\beta$ . Note also that, consistent with Theorem 1, we can quickly decrease this gap by increasing the value of  $\beta$ .

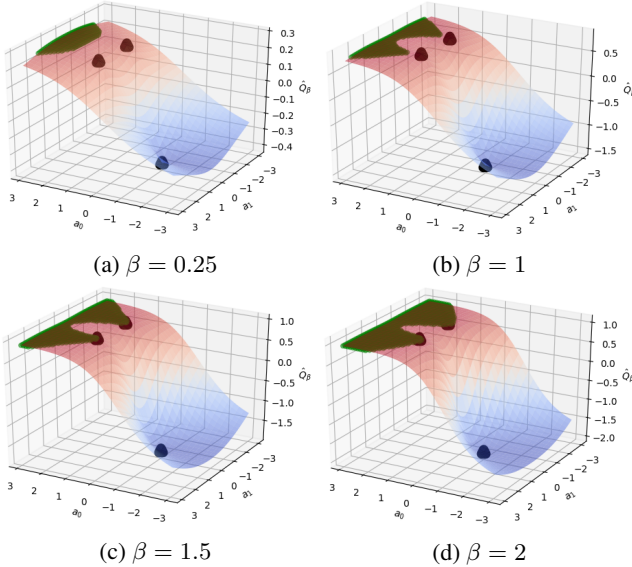


**Figure 2.** An RBF  $Q$  function with 3 fixed centroid locations and centroid values (shown as black dots), but different settings of the smoothing parameter  $\beta$  on a 2-dimensional action space. Green regions highlight the set of actions  $a$  for which  $a$  is extremely close to the global maximum, or more formally the set  $\{a \in \mathcal{A} \mid \max_{a \in \mathcal{A}} \{Q_\beta(s, a; \theta)\} - Q_\beta(s, a; \theta) < 0.02\}$ . Observe the fast reduction of the gap between  $\max_{a \in \mathcal{A}} \widehat{Q}_\beta(s, a; \theta)$  and  $\max_{i \in [1, N]} \widehat{Q}_\beta(s, a_i; \theta)$  by increasing  $\beta$ , as guaranteed by Theorem 1. Specifically,  $\max_{a \in \mathcal{A}} \widehat{Q}_\beta(s, a; \theta) - \max_{i \in [1, N]} \widehat{Q}_\beta(s, a_i; \theta) < 0.02$  for any  $\beta \geq 1.5$ . Also, observe that the function becomes less *smooth* as we increase  $\beta$ .

In light of the above theoretical result, to approximate  $\max_{a \in \mathcal{A}} \widehat{Q}(s, a; \theta)$  we compute  $\max_{i \in [1, N]} \widehat{Q}(s, a_i; \theta)$ . If the goal is to ensure that the approximation is sufficiently

accurate, one can always increase the smoothing parameter to quickly get the desired accuracy.

Notice that this result holds for normalized Gaussian RBF networks, but not necessarily for the unnormalized case or for other types of RBFs. We believe that this observation is an interesting result in and of itself, regardless of its connection to value-function-based RL.

We finally note that, for the case where we are actually interested in an approximation for  $\min_{a \in \mathcal{A}} \widehat{Q}_\beta(s, a; \theta)$ , we can get the following corollary akin to Theorem 1:

**Corollary.** Let  $\widehat{Q}_\beta$  be a member of the class of normalized Gaussian RBF value functions as formulated in (6).

• For  $\mathcal{A} = \mathcal{R}$ :

$$\min_{a \in \mathcal{A}} \widehat{Q}_\beta(s, a; \theta) = \min_{i \in [1, N]} \widehat{Q}_\beta(s, a_i; \theta).$$

• For  $\mathcal{A} = \mathcal{R}^d \quad \forall d \geq 1$ :

$$0 \leq \min_{i \in [1, N]} \widehat{Q}_\beta(s, a_i; \theta) - \min_{a \in \mathcal{A}} \widehat{Q}_\beta(s, a; \theta) \leq \mathcal{O}(e^{-\beta}).$$

We now move to the second desired property of RBF  $Q$  networks, namely that these networks are in fact capable of universal function approximation (UFA).

**Theorem 2.** Consider any state-action value function  $Q^\pi(s, a)$  defined on a closed action space  $\mathcal{A}$ . Assume that  $Q^\pi(s, a)$  is a continuous function. For a fixed state  $s$  and for any  $\epsilon > 0$ , there exists a deep RBF value function  $\widehat{Q}_\beta(s, a; \theta)$  and a setting of the smoothing parameter  $\beta_0$  for which:

$$\forall a \in \mathcal{A} \quad \forall \beta \geq \beta_0 \quad |Q^\pi(s, a) - \widehat{Q}_\beta(s, a; \theta)| \leq \epsilon.$$

*Proof.* See Appendix.  $\square$

Collectively, Theorems 1 and 2 guarantee that deep RBF  $Q$  functions preserve the desired UFA property while ensuring accurate and efficient action maximization. This combination of properties stands in contrast with prior work that used function classes that enable easy action maximization but lack the UFA property (Gu et al., 2016; Amos et al., 2017), as well as prior work that preserved the UFA property but did not guarantee arbitrarily low accuracy when performing the maximization step (Lim et al., 2018; Ryu et al., 2019). The only important assumption in Theorem 2 is that the true value function  $Q^\pi(s, a)$  is continuous, which is a standard assumption in the UFA literature (Hornik et al., 1989) and in RL (Asadi et al., 2018).

We note that, while using a large value of  $\beta$  makes it theoretically possible to approximate any function up to any

desired accuracy, there is a downside to using large  $\beta$  values. Specifically, very large values of  $\beta$  result in extremely *local* approximations, which ultimately increases sample complexity as experience is not generalized from centroid to centroid. The bias–variance tension between using large  $\beta$  values that allow for greater accuracy and using smaller  $\beta$  values that reduce sample complexity make intermediate values of  $\beta$  work best. This property could be examined formally through the lens of regularization (Bartlett & Mendelson, 2002).

As for scalability to large action spaces, note that the RBF formulation scales naturally owing to its freedom to come up with centroids that best minimize the loss function. As a thought experiment, suppose that some region of the action space has a high value, so an agent with greedy action selection frequently chooses actions from that region. The deep RBF  $Q$  function would then move more centroids to the region, because the region heavily contributes to the loss function. It is unnecessary, then, to initialize centroid locations carefully, or to uniformly cover the action space *a priori*. In our RL experiments in Section 5, we achieved reasonable results with the number of centroids fixed across every problem, indicating that we need not rapidly increase the number of centroids as the action dimension increases.

#### 4. Experiments: Continuous Optimization

To demonstrate the operation of an RBF network in the simplest and clearest setting, we start with a single-input continuous optimization problem, where the agent lacks access to the true reward function but can sample input–output pairs  $\langle a, r \rangle$ . This setting is akin to the action maximization step in RL for a single state or, stated differently, a continuous bandit problem. We are interested in evaluating approaches that use tuples of experience  $\langle a, r \rangle$  to learn the surface of the reward function, and then optimize the learned function.

To this end, we chose the reward function:

$$r(a) = \|a\|_2 \frac{\sin(a_0) + \sin(a_1)}{2}. \quad (7)$$

Figure 3 (left) shows the surface of this function. It is clearly non-convex and includes several local maxima (and minima). We are interested in two cases, first the problem where the goal is to find  $\max_a r(a)$ , and the converse problem where we desire to find  $\min_a r(a)$ .

Exploration is challenging in this setting (Lattimore & Szepesvári, 2018). Here, our focus is not to find the most effective exploration policy, but to evaluate different approaches based on their effectiveness to represent and optimize a learned reward function  $\hat{r}(a; \theta)$ . So, in the interest of fairness, we adopt the same random action-selection strategy for all approaches.

More concretely, we sampled 500 actions uniformly randomly from  $[-3, 3]^2$  and provided the agent with the reward associated with the actions according to (7). We then used this dataset for training. When learning ended, we computed the action that maximized (or minimized) the learned  $\hat{r}(a; \theta)$ . Details of the function classes used in each case, as well as how to perform  $\max_a \hat{r}(a; \theta)$  and  $\min_a \hat{r}(a; \theta)$  will now be presented below for each individual approach.

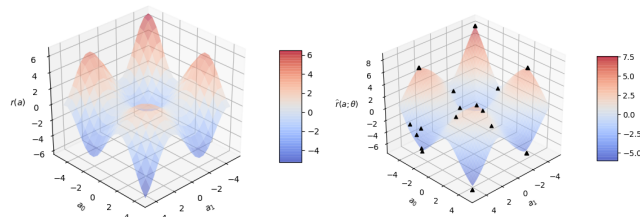


Figure 3. Left: Surface of the true reward function. Right: The surface learned by the RBF reward network in a sample run. Black dots represent the centroids.

For our first baseline, we discretized each action dimension to 7 bins, resulting in 49 bins that uniformly covered the two dimensions of the input space. For each bin, we averaged the rewards over  $\langle a, r \rangle$  pairs for which the sampled action  $a$  belonged to that bin. Once we had a learned  $\hat{r}(a; \theta)$ , which in this case was just a  $7 \times 7$  table, we performed  $\max_a \hat{r}(a; \theta)$  and  $\min_a \hat{r}(a; \theta)$  by a simple table lookup. Discretization clearly fails to scale to problems with higher dimensionality, and we have included this baseline solely for completeness.

Our second baseline used the input-convex neural network architecture (Amos et al., 2017), where the neural network is constrained so that the learned reward function  $\hat{r}(a; \theta)$  is convex. Learning was performed by RMSProp optimization (Goodfellow et al., 2016) with mean-squared loss. Once  $\hat{r}(a; \theta)$  was learned, we used gradient ascent for finding the maximum, and gradient descent for finding the minimum. Note that this input-convex approach subsumes the excluded quadratic case proposed by Gu et al. (2016), because quadratic functions are just a special case of convex functions, but the converse is not necessarily true (Boyd & Vandenberghe, 2004).

Our next baseline was the wire-fitting method proposed by Baird & Klopff (1993). This method is similar to RBF networks in that it also learns a set of centroids. Similar to the previous case, we used the RMSprop optimizer and mean-squared loss, and finally returned the centroids with lowest (or highest) values according to the learned  $\hat{r}(a; \theta)$ .

As the last baseline, we used a standard feed-forward neural network architecture with two hidden layers to learn  $\hat{r}(a; \theta)$ . It is well-known that this function class is capable of UFA (Hornik et al., 1989) and so can accurately

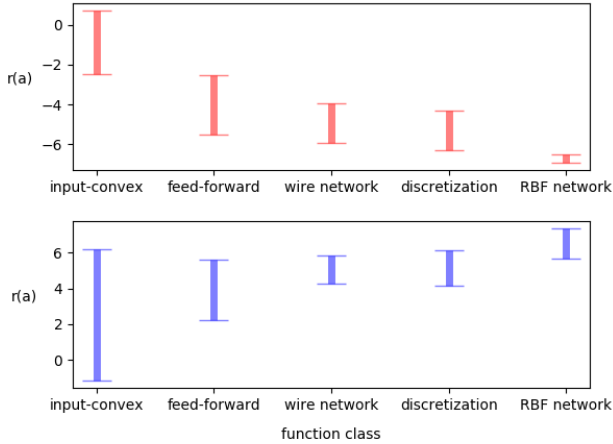


Figure 4. Mean and standard deviation of performance for various methods on the continuous optimization task. Here,  $r(a)$  denotes the true reward associated with the action  $a$  found by each method. Top: Results for action minimization. (Lower is better.) Bottom: Results for action maximization. (Higher is better.) Results are averaged over 30 independent runs. The RBF architecture outperforms the alternatives in both cases.

learn the reward function in principle. However, once learning ends, we face a non-convex optimization problem for action maximization (or minimization)  $\max_a \hat{r}(a; \theta)$ . We simply initialized gradient descent (ascent) to a point chosen uniformly randomly, and followed the corresponding direction until convergence.

To learn an RBF reward function, we used  $N = 50$  centroids and  $\beta = 0.5$ . We again used RMSprop and mean-squared loss minimization. Recall that Theorem 1 showed that with an RBF network the following approximations are well-justified in theory:  $\max_{a \in \mathcal{A}} \hat{r}(a) \approx \max_{i \in [1, 50]} \hat{r}(a_i)$  and  $\min_{a \in \mathcal{A}} \hat{r}(a) \approx \min_{i \in [1, 50]} \hat{r}(a_i)$ . As such, when the learning of  $\hat{r}(a; \theta)$  ends, we output the centroid values with highest and lowest reward.

For each individual case, we ran the corresponding experimental pipeline for 30 different random seeds. The solution found by each learner was fed to the true reward function (7) to get the true quality of the found solution. We report the average reward achieved by each function class in Figure 4. The RBF learner outperforms all baselines on both the maximization and the minimization problem. We further show the function learned by a sample run of RBF on the right side of Figure 3, which is an almost perfect approximation for the true reward function.

## 5. Experiments: Continuous Control

We now use deep  $Q$  functions for solving continuous-action RL problems. To this end, we learn a deep RBF  $Q$  function using a learning algorithm similar to that of DQN (Mnih

et al., 2015), but extended to the continuous-action case. DQN uses the following loss function for learning a deep state-action value function:

$$L(\theta) := \mathbf{E}_{s,a,r,s'} \left[ (r + \gamma \max_{a' \in \mathcal{A}} \hat{Q}(s', a'; \theta^-) - \hat{Q}(s, a; \theta))^2 \right].$$

DQN adds tuples of experience  $\langle s, a, r, s' \rangle$  to a buffer, and later samples a minibatch of tuples to compute  $\nabla_{\theta} L(\theta)$ . DQN maintains a second network parameterized by weights  $\theta^-$ . This second network, denoted  $\hat{Q}(\cdot, \cdot, \theta^-)$  and referred to as the target network, is periodically synchronized with the online network  $\hat{Q}(\cdot, \cdot, \theta)$ .

---

### Algorithm 1 Pseudocode for RBF-DQN

---

```

Initialize RBF network architecture with  $N$  centroids
RBF smoothing parameter  $\beta$ 
RBF online network parameters  $\theta$  and  $\theta^-$ 
optimizer learning rate  $\alpha_{\theta}$ 
target network learning rate  $\alpha_{\theta^-}$ 
total training episodes  $E$ , minibatch size  $M$ 
discount rate  $\gamma$ , replay buffer  $\mathcal{B}$ , decay rate  $\mu$ 
for episode  $\in [1, E]$  do
   $s \leftarrow \text{env.reset}()$ , done  $\leftarrow \text{False}$ ,  $\epsilon \leftarrow (1 + \text{episode})^{-\mu}$ 
  while done==False do
     $a \leftarrow \epsilon\text{-greedy}(\hat{Q}_{\beta}(\cdot, \cdot; \theta), s, \epsilon)$ 
     $s', r$ , done  $\leftarrow \text{env.step}(s, a)$ 
    add  $\langle s, a, r, s', \text{done} \rangle$  to  $\mathcal{B}$ 
     $s \leftarrow s'$ 
  end while
  for  $M$  minibatches sampled from  $\mathcal{B}$  do
     $\Delta_m^{\theta} = (r - \hat{Q}_{\beta}(s, a; \theta)) \nabla_{\theta} \hat{Q}(s, a; \theta)$ 
    if done==False then
      get centroids  $a'_i(s; \theta^-) \forall i \in [1, N]$ 
       $\Delta_m^{\theta} += \gamma \max_{a'_i} \hat{Q}_{\beta}(s', a'_i; \theta^-) \nabla_{\theta} \hat{Q}_{\beta}(s, a; \theta)$ 
    end if
  end for
   $\Delta^{\theta} \leftarrow \frac{\sum_{m=1}^M \Delta_m^{\theta}}{M}$ 
   $\theta \leftarrow \text{RMSProp}(\theta, \Delta^{\theta}, \alpha_{\theta})$ 
   $\theta^- \leftarrow (1 - \alpha_{\theta^-})\theta^- + \alpha_{\theta^-}\theta$ 
end for
function  $\epsilon\text{-greedy}(\hat{Q}_{\beta}, s, \epsilon)$ :
  temp  $\sim$  uniformly from  $[0, 1]$ 
if temp  $\leq \epsilon$  then
     $a \sim$  uniformly from  $\mathcal{A}$ 
    return  $a$ 
else
  get centroids  $a_i(s; \theta) \forall i \in [1, N]$ 
  return  $\arg \max_{a_i} \hat{Q}_{\beta}(s, a_i; \theta)$ 
end if

```

---

RBF-DQN uses the same loss function, but modifies the function class of DQN. Concretely, DQN learns a deep network that outputs a scalar action-value output per action,

exploiting the discrete and finite nature of the action space. By contrast, RBF-DQN takes a state vector and an action vector as input, and outputs a single scalar using a deep RBF  $Q$  function. Note that every operation in a deep RBF  $Q$  function is differentiable, so the gradient of the loss function with respect to  $\theta$  parameters can be computed using standard deep learning libraries. Specifically, we used Python’s Tensorflow library (Abadi et al., 2016) with Keras (Chollet, 2015) as its interface.

In terms of action selection, with probability  $\epsilon$ , DQN chooses a random action, and with probability  $1 - \epsilon$  it chooses an action with the highest value. The value of  $\epsilon$  is annealed so that the agent becomes more greedy as learning proceeds. To define an analog of this so called  $\epsilon$ -greedy policy for RBF-DQN, we sample from a uniform distribution with probability  $\epsilon$ , and we take  $\arg \max_{i \in [1, N]} \hat{Q}_\beta(s, a_i; \theta)$  with probability  $1 - \epsilon$ . We annealed the  $\epsilon$  parameter, similar to DQN.

Additionally, we made a minor change to the original DQN algorithm in terms of updating  $\theta^-$ , the weights of the target network. Concretely, we update  $\theta^-$  using an exponential moving average of all the previous  $\theta$  values, as suggested by Lillicrap et al. (2015):  $\theta^- \leftarrow (1 - \alpha)\theta^- + \alpha\theta$ , which differs from the occasional periodic updates  $\theta^- \leftarrow \theta$  of the original DQN agent. We observed a significant performance increase with this simple modification.

For completeness, we provide pseudocode for RBF-DQN in Algorithm 1, include the code for the algorithm in the supplementary material, and will provide an open repository<sup>1</sup>.

We compared RBF-DQN’s performance to other deep-RL baselines on a large set of standard continuous-action RL domains from Gym (Brockman et al., 2016). These domains range from simple tasks such as Inverted Pendulum with a one-dimensional action space, to more complicated domains such as Ant with a 7-dimensional action space. We used the same number of centroids  $N = 30$  for learning the deep RBF  $Q$  function. We found the performance of RBF-DQN to be most sensitive to two hyper-parameters, namely RMSProp’s learning rate  $\alpha_\theta$  and the RBF smoothing parameter  $\beta$ . We tuned these two parameters via grid search (Goodfellow et al., 2016) for each individual domain, while all other hyperparameters were fixed across domains. See the Appendix for a complete explanation of the process of hyper-parameter tuning for RBF-DQN, as well as for the baselines.

For a meaningful comparison, we performed roughly similar numbers of gradient-based updates for RBF-DQN and the baselines. Specifically, in all domains, we performed  $M = 100$  updates per episode on RBF-DQN’s network

parameters  $\theta$ . We used the same number of updates per episode for other value-function-based baselines, such as input-convex neural networks (Amos et al., 2017). Moreover, in the case of policy-gradient baseline DDPG (Lillicrap et al., 2015), we performed 100 value-function updates and 100 policy updates per episode. This number of updates gave us reasonable results in terms of data efficiency, and it also helped us run all experiments on modern CPUs.

In choosing our baselines, our main goal was to compare RBF-DQN to other value-function-based deep-RL baselines that explicitly perform the maximization step. We did not perform comparisons with an exhaustive set of existing policy gradient methods from the literature, since they work fundamentally differently than RBF-DQN and circumvent the action-maximization step. That said, deep deterministic policy gradient (DDPG) (Lillicrap et al., 2015) and its more advanced variant, TD3 (Fujimoto et al., 2018), are two very common baselines in continuous control, so we included them for completeness.

Moreover, in light of recent concerns with reproducibility in RL (Henderson et al., 2018), we ran each algorithm for 10 fixed random seeds and report average performance, we release our code, and we clearly explain our hyper-parameter tuning process in the Appendix. Other than the input-convex neural network baseline (Amos et al., 2017), for which the authors released Tensorflow code, we chose to implement RBF-DQN and all other baselines ourselves and in Tensorflow. This choice reflected a concern that comparing results across different deep-learning libraries is extremely difficult.

It is clear from Figure 5 that RBF-DQN is competitive to all baselines both in terms of data efficiency and final performance. Moreover, we report final mean-performance with standard errors in the Appendix. RBF-DQN yields the highest-performing final policies in 8 out of the 9 domain.

## 6. Future Work

We envision several promising directions for future work. First, the RL literature has numerous examples of algorithmic ideas that help improve value-function-based agents (see Hessel et al. (2018) for some examples). These ideas are usually proposed for domains with discrete actions, so extending them to continuous-action domains using RBF-DQN could be an exciting direction to pursue.

A big advantage of value-function-based methods is the flexibility that they offer when tackling the exploration problem. Examples of exploration strategies for these methods include optimistic initialization (Sutton & Barto, 2018), softmax policies (Rummery & Niranjan, 1994; Sutton & Barto, 2018), uncertainty-based exploration (Osband et al., 2016), and PAC learning (Kakade, 2003;

<sup>1</sup>github.com/kavosh8/RBFDQN

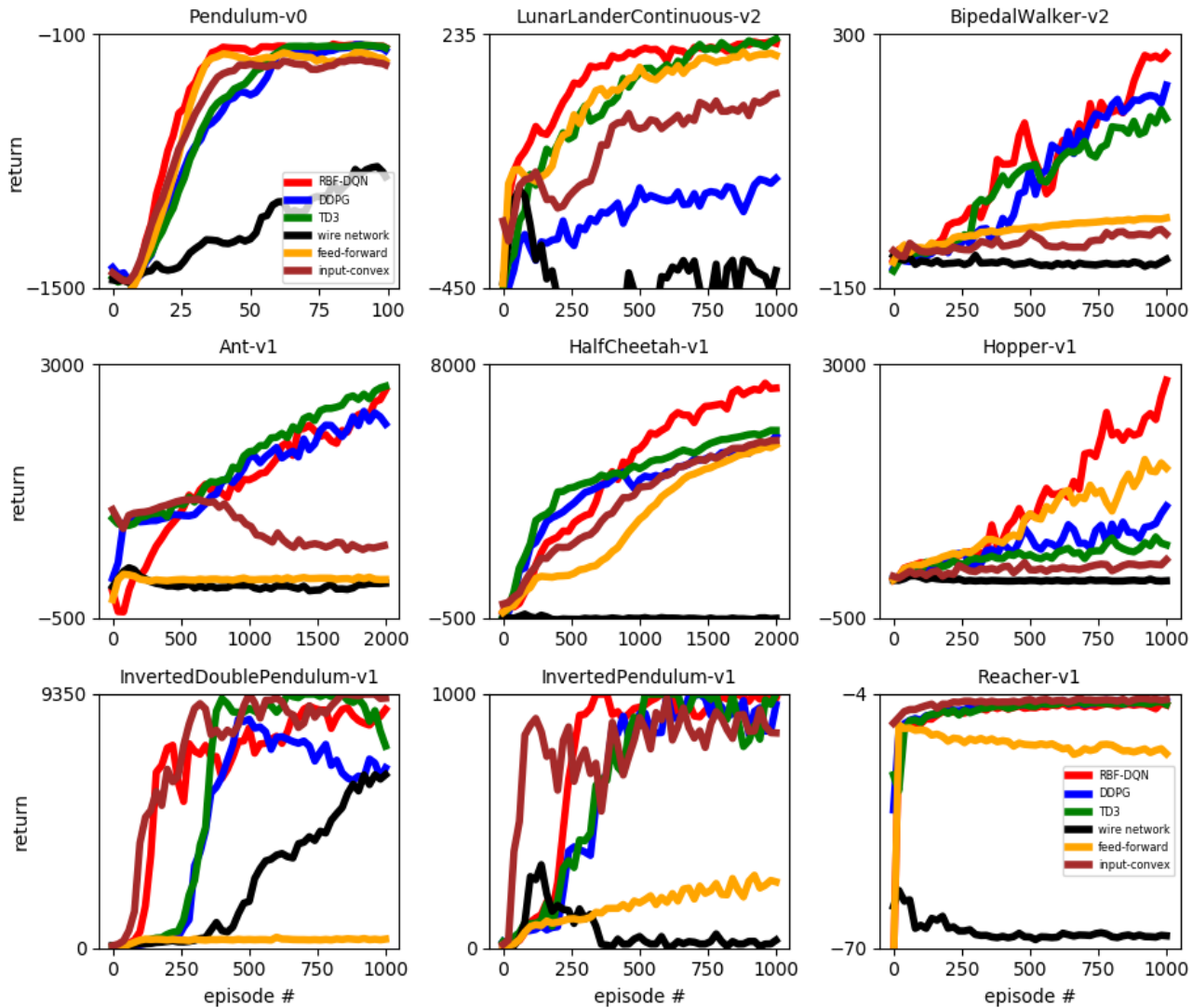


Figure 5. A comparison between RBF-DQN and baselines on continuous-action RL domains. Y-axis shows sum of rewards across each episode, so higher is better. In the Appendix, we compare these agents based on mean and standard error of their final performance.

Strehl et al., 2006). We used a simple  $\epsilon$ -greedy policy, but a combination of the advanced exploration strategies with deep RBF  $Q$  functions could be more effective.

Moreover, we solely focused on deep RBF value functions with negative exponentials, but various RBFs exist in the literature (Karayiannis, 1999). Further research into other types of RBFs can shed light on their strengths and weaknesses in the context of continuous-action RL problems. Moreover, we noticed that tuning the smoothing parameter of negative exponentials can be challenging, so methods that automatically learn this parameter, such as meta gradient approaches (Xu et al., 2018), are a promising direction for future.

Finally, we look forward to applying deep RBF  $Q$  functions

to key problems, such as robotics, real-time bidding, recommendation systems, and dialog systems.

## 7. Conclusion

We proposed, analyzed, and exhibited the strengths of deep RBF value functions in continuous control. These value functions facilitate easy action maximization, support universal function approximation, and scale to large continuous action spaces. Deep RBF value functions are thus an appealing choice for value function approximation in continuous control.



## References

- Abadi, M., Barham, P., Chen, J., Chen, Z., Davis, A., Dean, J., Devin, M., Ghemawat, S., Irving, G., Isard, M., et al. Tensorflow: A system for large-scale machine learning. In *12th USENIX Symposium on Operating Systems Design and Implementation*, pp. 265–283, 2016.
- Amos, B., Xu, L., and Kolter, J. Z. Input convex neural networks. In *Proceedings of the 34th International Conference on Machine Learning*, pp. 146–155, 2017.
- Asadi, K. and Littman, M. L. An alternative softmax operator for reinforcement learning. In *Proceedings of the 34th International Conference on Machine Learning*, pp. 243–252, 2017.
- Asadi, K., Misra, D., and Littman, M. L. Lipschitz continuity in model-based reinforcement learning. In *Proceedings of the 35th International Conference on Machine Learning*, pp. 264–273, 2018.
- Aurenhammer, F. Voronoi diagrams—a survey of a fundamental geometric data structure. *ACM Computing Surveys*, 23(3):345–405, 1991.
- Baird, L. C. and Klopff, A. H. Reinforcement learning with high-dimensional, continuous actions. Technical report, 1993.
- Bartlett, P. L. and Mendelson, S. Rademacher and Gaussian complexities: Risk bounds and structural results. *Journal of Machine Learning Research*, 3(Nov):463–482, 2002.
- Bellman, R. On the theory of dynamic programming. *Proceedings of the National Academy of Sciences of the United States of America*, 38(8):716, 1952.
- Benaim, M. On functional approximation with normalized Gaussian units. *Neural Computation*, 6(2):319–333, 1994.
- Boyd, S. and Vandenberghe, L. *Convex optimization*. Cambridge University Press, 2004.
- Brockman, G., Cheung, V., Pettersson, L., Schneider, J., Schulman, J., Tang, J., and Zaremba, W. OpenAI Gym. *arXiv preprint arXiv:1606.01540*, 2016.
- Broomhead, D. S. and Lowe, D. Radial basis functions, multi-variable functional interpolation and adaptive networks. Technical report, 1988.
- Bugmann, G. Normalized Gaussian radial basis function networks. *Neurocomputing*, 20(1-3):97–110, 1998.
- Chollet, F. keras. <https://github.com/fchollet/keras>, 2015.
- Fujimoto, S., Hoof, H., and Meger, D. Addressing function approximation error in actor-critic methods. In *International Conference on Machine Learning*, pp. 1587–1596, 2018.
- Goodfellow, I., Bengio, Y., and Courville, A. *Deep learning*. MIT press, 2016.
- Gu, S., Lillicrap, T., Sutskever, I., and Levine, S. Continuous deep Q-learning with model-based acceleration. In *International Conference on Machine Learning*, pp. 2829–2838, 2016.
- Hammer, B. and Gersmann, K. A note on the universal approximation capability of support vector machines. *Neural Processing Letters*, 17(1):43–53, 2003.
- Henderson, P., Islam, R., Bachman, P., Pineau, J., Precup, D., and Meger, D. Deep reinforcement learning that matters. In *Proceedings of the Thirty-Second AAAI Conference on Artificial Intelligence*, 2018.
- Hessel, M., Modayil, J., Van Hasselt, H., Schaul, T., Ostrovski, G., Dabney, W., Horgan, D., Piot, B., Azar, M., and Silver, D. Rainbow: Combining improvements in deep reinforcement learning. In *Proceedings of the Thirty-Second AAAI Conference on Artificial Intelligence*, 2018.
- Hornik, K., Stinchcombe, M., and White, H. Multilayer feedforward networks are universal approximators. *Neural networks*, 2(5):359–366, 1989.
- Kakade, S. *On the sample complexity of reinforcement learning*. PhD thesis, University of London London, England, 2003.
- Kakade, S. and Langford, J. Approximately optimal approximate reinforcement learning. In *Proceedings of the International Conference on Machine Learning*, pp. 267–274, 2002.
- Karayiannis, N. B. Reformulated radial basis neural networks trained by gradient descent. *IEEE Transactions on Neural Networks*, 10(3):657–671, 1999.
- Kingma, D. P. and Ba, J. Adam: A method for stochastic optimization. *arXiv preprint arXiv:1412.6980*, 2014.
- Konidaris, G., Osentoski, S., and Thomas, P. Value function approximation in reinforcement learning using the Fourier basis. In *Proceedings of the Twenty-Fifth AAAI Conference on Artificial Intelligence*, 2011.
- Lattimore, T. and Szepesvári, C. Bandit algorithms. *preprint*, 2018.

- Lillicrap, T. P., Hunt, J. J., Pritzel, A., Heess, N., Erez, T., Tassa, Y., Silver, D., and Wierstra, D. Continuous control with deep reinforcement learning. *arXiv preprint arXiv:1509.02971*, 2015.
- Lim, S., Joseph, A., Le, L., Pan, Y., and White, M. Actor-expert: A framework for using action-value methods in continuous action spaces. *arXiv preprint arXiv:1810.09103*, 2018.
- Matheron, G., Perrin, N., and Sigaud, O. The problem with DDPG: understanding failures in deterministic environments with sparse rewards. *arXiv preprint arXiv:1911.11679*, 2019.
- Mnih, V., Kavukcuoglu, K., Silver, D., Rusu, A. A., Veness, J., Bellemare, M. G., Graves, A., Riedmiller, M., Fidjeland, A. K., Ostrovski, G., et al. Human-level control through deep reinforcement learning. *Nature*, 518 (7540):529, 2015.
- Moody, J. and Darken, C. J. Fast learning in networks of locally-tuned processing units. *Neural computation*, 1(2): 281–294, 1989.
- Osband, I., Blundell, C., Pritzel, A., and Van Roy, B. Deep exploration via bootstrapped DQN. In *Advances in neural information processing systems*, pp. 4026–4034, 2016.
- Powell, M. J. Radial basis functions for multivariable interpolation: a review. *Algorithms for approximation*, 1987.
- Puterman, M. L. *Markov Decision Processes.: Discrete Stochastic Dynamic Programming*. John Wiley & Sons, 2014.
- Rummery, G. A. and Niranjan, M. *On-line Q-learning using connectionist systems*, volume 37. University of Cambridge, Department of Engineering Cambridge, England, 1994.
- Ryu, M., Chow, Y., Anderson, R., Tjandraatmadja, C., and Bouillier, C. Caql: Continuous action q-learning. *arXiv preprint arXiv:1909.12397*, 2019.
- Silver, D., Lever, G., Heess, N., Degris, T., Wierstra, D., and Riedmiller, M. Deterministic policy gradient algorithms. In *International Conference on Machine Learning*, pp. 387–395, 2014.
- Song, Z., Parr, R., and Carin, L. Revisiting the softmax bellman operator: New benefits and new perspective. In *International Conference on Machine Learning*, pp. 5916–5925, 2019.
- Strehl, A. L., Li, L., Wiewiora, E., Langford, J., and Littman, M. L. PAC model-free reinforcement learning. In *Proceedings of the 23rd International Conference on Machine Learning*, pp. 881–888, 2006.
- Sutton, R. S. Learning to predict by the methods of temporal differences. *Machine Learning*, 3(1):9–44, 1988.
- Sutton, R. S. Generalization in reinforcement learning: Successful examples using sparse coarse coding. In *Advances in Neural Information Processing Systems*, pp. 1038–1044, 1996.
- Sutton, R. S. and Barto, A. G. *Reinforcement learning: An introduction*. MIT press, 2018.
- Watkins, C. Learning from delayed rewards. *King’s College, Cambridge*, 1989.
- Xu, Z., van Hasselt, H. P., and Silver, D. Meta-gradient reinforcement learning. In *Advances in Neural Information Processing Systems*, pp. 2396–2407, 2018.

## 8. Appendix

### 8.1. Proofs

**Theorem 1.** Let  $\widehat{Q}_\beta$  be a member of the class of normalized Gaussian RBF value functions.

I) For a one-dimensional action space  $\mathcal{A} = \mathcal{R}$ :

$$\max_{a \in \mathcal{A}} \widehat{Q}_\beta(s, a; \theta) = \max_{i \in [1, N]} \widehat{Q}_\beta(s, a_i; \theta).$$

II) For  $\mathcal{A} = \mathcal{R}^d \quad \forall d \geq 1$ :

$$0 \leq \max_{a \in \mathcal{A}} \widehat{Q}_\beta(s, a; \theta) - \max_{i \in [1, N]} \widehat{Q}_\beta(s, a_i; \theta) \leq \mathcal{O}(e^{-\beta}).$$

*Proof.* We begin by proving the first result. For an arbitrary action  $a$ , we can write:

$$\widehat{Q}_\beta(s, a; \theta) = w_1 v_1(s; \theta) + \dots + w_N v_N(s; \theta),$$

where each weight  $w_i$  is determined via softmax. Without loss of generality, we sort all anchor points so that  $\forall i \ a_i < a_{i+1}$ . Take two neighboring centroids  $a_L$  and  $a_R$  and notice that:

$$\forall i < L, \quad \frac{w_L}{w_i} = \frac{e^{-|a-a_L|}}{e^{-|a-a_i|}} = \frac{e^{-a+a_L}}{e^{-a+a_i}} = e^{a_L-a_i} \stackrel{\text{def}}{=} \frac{1}{c_i} \implies w_i = w_L c_i.$$

In the above, we used the fact that all  $a_i$  are to the left of  $a$  and  $a_L$ . Similarly, we can argue that  $\forall i > R \ W_i = W_R c_i$ . Intuitively, as long as the action is between  $a_L$  and  $a_R$ , the ratio of the weight of a centroid to the left of  $a_L$ , over the weight of  $a_L$  itself, remains constant and does not change with  $a$ . The same holds for the centroids to the right of  $a_R$ . In light of the above result, by renaming some variables we can now write:

$$\begin{aligned} \widehat{Q}_\beta(s, a; \theta) &= w_1 v_1(s; \theta) + \dots + w_L v_L(s; \theta) + w_R v_R(s; \theta) + \dots + w_K v_K(s; \theta) \\ &= w_L c_1 v_1(s; \theta) + \dots + w_L v_L(s; \theta) + w_R v_R(s; \theta) + \dots + w_R c_K v_K(s; \theta) \\ &= w_L (c_1 v_1(s; \theta) + \dots + v_L(s; \theta)) + w_R (v_R(s; \theta) + \dots + c_K v_K(s; \theta)). \end{aligned}$$

Moreover, note that the weights need to sum up to 1:

$$w_L(c_1 + \dots + 1) + w_R(1 + \dots + c_K) = 1, \quad ,$$

and  $w_L$  is at its peak when we choose  $a = a_L$  and at its smallest value when we choose  $a = a_R$ . A converse statement is true about  $w_R$ . Moreover, the weights monotonically increase and decrease as we move the input  $a$ . We call the endpoints of the range  $w_{min}$  and  $w_{max}$ . As such, the problem  $\max_{a \in [a_L, a_R]} \widehat{Q}_\beta(s, a; \theta)$  could be written as this linear program:

$$\begin{aligned} \max_{w_L, w_R} \quad & w_L (c_1 v_1(s; \theta) + \dots + v_L(s; \theta)) + w_R (v_R(s; \theta) + \dots + c_K v_K(s; \theta)) \\ \text{s.t.} \quad & w_L (c_1 + \dots + 1) + w_R (1 + \dots + c_K) = 1 \\ & w_L, w_R \geq W_{min} \\ & w_L, w_R \leq W_{max} \end{aligned}$$

A standard result in linear programming is that every linear program has an extreme point that is an optimal solution (Boyd & Vandenberghe, 2004). Therefore, at least one of the points  $(w_L = w_{min}, w_R = w_{max})$  or  $(w_L = w_{max}, w_R = w_{min})$  is an optimal solution. It is easy to see that there is a one-to-one mapping between  $a$  and  $W_L, W_R$  in light of the monotonic property. As a result, the first point corresponds to the unique value of  $a = a_R(s)$ , and the second corresponds to unique value of  $a = a_L(s)$ . Since no point in between two centroids can be bigger than the surrounding centroids, at least one of the centroids is a globally optimal solution in the range  $[a_1(s), a_N(s)]$ , that is

$$\max_{a \in [a_1(s; \theta), a_N(s; \theta)]} \widehat{Q}_\beta(s, a; \theta) = \max_{a_i} \widehat{Q}_\beta(s, a_i; \theta).$$

To finish the proof, we can show that  $\forall a < a_1 \widehat{Q}_\beta(s, a; \theta) = \widehat{Q}_\beta(s, a_1; \theta)$ . The proof for  $\forall a > a_N \widehat{Q}_\beta(s, a; \theta) = \widehat{Q}_\beta(s, a_N; \theta)$  follows similar steps. So,

$$\begin{aligned}
 \forall a < a_1 \widehat{Q}_\beta(s, a; \theta) &= \frac{\sum_{i=1}^N e^{-\beta|a-a_i(s)|} v_i(s)}{\sum_{i=1}^N e^{-\beta|a-a_i(s)|}} \\
 &= \frac{\sum_{i=1}^N e^{-\beta|a_1-c-a_i(s)|} v_i(s)}{\sum_{i=1}^N e^{-\beta|a_1-c-a_i(s)|}} \\
 &= \frac{\sum_{i=1}^N e^{\beta(a_1-c-a_i(s))} v_i(s)}{\sum_{i=1}^N e^{\beta(a_1-c-a_i(s))}} \\
 &= \frac{e^{-c} \sum_{i=1}^N e^{\beta(a_1-a_i(s))} v_i(s)}{e^{-c} \sum_{i=1}^N e^{\beta(a_1-a_i(s))}} \\
 &= \frac{\sum_{i=1}^N e^{\beta(a_1-a_i(s))} v_i(s)}{\sum_{i=1}^N e^{\beta(a_1-a_i(s))}} = \widehat{Q}_\beta(s, a_1; \theta),
 \end{aligned}$$

which concludes the proof of the first part.

We now move to the more general case with  $\mathcal{A} = \mathcal{R}^m$ :

$$\begin{aligned}
 \max_a \widehat{Q}_\beta(s, a; \theta) - \max_{i \in \{1:N\}} \widehat{Q}(s, a_i; \theta) &\leq v_{max}(s; \theta) - \max_{i \in \{1:N\}} \widehat{Q}(s, a_i; \theta) \\
 &\leq v_{max}(s; \theta) - \widehat{Q}_\beta(s, a_{max}; \theta).
 \end{aligned}$$

WLOG, we assume the first centroid is the one with highest  $v$ , that is  $v_1(s; \theta) = \arg \max_{v_i} v_i(s; \theta)$ , and conclude the proof. Note that a related result was shown recently (Song et al., 2019):

$$\begin{aligned}
 v_{max}(s) - \widehat{Q}_\beta(s, a_{max}; \theta) &= v_1 - \frac{\sum_{i=1}^N e^{-\beta\|a_1-a_i(s)\|} v_i(s)}{\sum_{i=1}^N e^{-\beta\|a_1-a_i(s)\|}} \\
 &= \frac{\sum_{i=1}^N e^{-\beta\|a_1-a_i(s)\|} (v_1(s) - v_i(s))}{\sum_{i=1}^N e^{-\beta\|a_1-a_i(s)\|}} \\
 &= \frac{\sum_{i=2}^N e^{-\beta\|a_1-a_i(s)\|} (v_1(s) - v_i(s))}{1 + \sum_{k=2}^K e^{-\beta\|a_1-a_i(s)\|}} \\
 &\leq \Delta_q \frac{\sum_{i=2}^N e^{-\beta\|a_1-a_i(s)\|}}{1 + \sum_{i=2}^N e^{-\beta\|a_1-a_i(s)\|}} \\
 &\leq \Delta_q \sum_{i=2}^N \frac{e^{-\beta\|a_1-a_i(s)\|}}{1 + e^{-\beta\|a_1-a_i(s)\|}} \\
 &= \Delta_q \sum_{i=2}^N \frac{1}{1 + e^{\beta\|a_1-a_i(s)\|}} = \mathcal{O}(e^{-\beta}).
 \end{aligned}$$

□

**Theorem 2.** Consider any state–action value function  $Q^\pi(s, a)$  defined on a closed action space  $\mathcal{A}$ . Assume that  $Q^\pi(s, a)$  is a continuous function. For a fixed state  $s$  and for any  $\epsilon > 0$ , there exists a deep RBF value function  $\widehat{Q}_\beta(s, a; \theta)$  and a setting of the smoothing parameter  $\beta_0$  for which:

$$\forall a \in \mathcal{A} \quad \forall \beta \geq \beta_0 \quad |Q^\pi(s, a) - \widehat{Q}_\beta(s, a; \theta)| \leq \epsilon.$$

*Proof.* Since  $Q^\pi$  is continuous, we leverage the fact that it is Lipschitz with a Lipschitz constant  $L$ :

$$\forall a_0, a_1 \quad |f(a_1) - f(a_0)| \leq L \|a_1 - a_0\|$$

As such, assuming that  $\|a_1 - a_0\| \leq \frac{\epsilon}{4L}$ , we have that

$$|f(a_1) - f(a_0)| \leq \frac{\epsilon}{4} \quad (8)$$

Consider a set of centroids  $\{c_1, c_2, \dots, c_N\}$ , define the  $cell(j)$  as:

$$cell(j) = \{a \in \mathcal{A} \mid \|a - c_j\| = \min_z \|a - c_z\|\},$$

and the radius  $Rad(j, \mathcal{A})$  as:

$$Rad(j, \mathcal{A}) := \sup_{x \in cell(j)} \|x - c_j\|.$$

Assuming that  $\mathcal{A}$  is a closed set, there always exists a set of centroids  $\{c_1, c_2, \dots, c_N\}$  for which  $Rad(c, \mathcal{A}) \leq \frac{\epsilon}{4L}$ . Now consider the following functional form:

$$\begin{aligned} \widehat{Q}_\beta(s, a) &:= \sum_{j=1}^N Q^\pi(s, c_j) w_j, \\ \text{where } w_j &= \frac{e^{-\beta \|a - c_j\|}}{\sum_{z=1}^N e^{-\beta \|a - c_z\|}}. \end{aligned}$$

Now suppose  $a$  lies in a subset of cells, called the *central* cells  $\mathcal{C}$ :

$$\mathcal{C} := \{j \mid a \in cell(j)\},$$

We define a second *neighboring* set of cells:

$$\mathcal{N} := \{j \mid cell(j) \cap (\cup_{i \in \mathcal{C}} cell(i)) \neq \emptyset\} - \mathcal{C},$$

and a third set of *far* cells:

$$\mathcal{F} := \{j \mid j \notin \mathcal{C} \ \& \ j \notin \mathcal{N}\},$$

We now have:

$$\begin{aligned} |Q^\pi(s, a) - \widehat{Q}_\beta(s, a; \theta)| &= \left| \sum_{j=1}^N (Q^\pi(s, a) - Q^\pi(s, c_j)) w_j \right| \\ &\leq \sum_{j=1}^N |Q^\pi(s, a) - Q^\pi(s, c_j)| w_j \\ &= \sum_{j \in \mathcal{C}} |Q^\pi(s, a) - Q^\pi(s, c_j)| w_j + \sum_{j \in \mathcal{N}} |Q^\pi(s, a) - Q^\pi(s, c_j)| w_j + \sum_{j \in \mathcal{F}} |Q^\pi(s, a) - Q^\pi(s, c_j)| w_j \end{aligned}$$

We now bound each of the three sums above. Starting from the first sum, it is easy to see that  $|Q^\pi(s, a) - Q^\pi(s, c_j)| \leq \frac{\epsilon}{4}$ , simply because  $a \in cell(j)$ . As for the second sum, since  $c_j$  is the centroid of a neighboring cell, using a central cell  $i$ , we can write:

$$\|a - c_j\| = \|a - c_i + c_i - c_j\| \leq \|a - c_i\| + \|c_i - c_j\| \leq \frac{\epsilon}{4L} + \frac{\epsilon}{4L} = \frac{\epsilon}{2L},$$

and so in this case  $|Q^\pi(s, a) - \widehat{Q}_\beta(s, c_j)| \leq \frac{\epsilon}{2}$ . In the third case with the set of far cells  $\mathcal{F}$ , observe that for a far cell  $j$  and a central cell  $i$  we have:

$$\frac{w_j}{w_i} = \frac{e^{-\beta \|a - c_j\|}}{e^{-\beta \|a - c_i\|}} \rightarrow w_j = w_i e^{-\beta(\|a - c_j\| - \|a - c_i\|)} \leq w_i e^{-\beta \mu} \leq e^{-\beta \mu},$$

For some  $\mu > 0$ . In the above, we used the fact that  $\|a - c_j\| - \|a - c_i\| > 0$  is always true.

Putting it all together, we have:

$$\begin{aligned}
 & |Q^\pi(s, a) - \widehat{Q}_\beta(s, a)| \\
 = & \sum_{j \in \mathcal{C}} \underbrace{|Q^\pi(s, a) - Q^\pi(s, c_j)|}_{\leq \frac{\epsilon}{4}} \underbrace{w_j}_{\leq 1} + \sum_{j \in \mathcal{N}} \underbrace{|Q^\pi(s, a) - Q^\pi(s, c_j)|}_{\leq \frac{\epsilon}{2}} \underbrace{w_j}_1 + \sum_{j \in \mathcal{F}} |Q^\pi(s, a) - Q^\pi(s, c_j)| \underbrace{w_j}_{e^{-\beta\mu}} \\
 \leq & \frac{\epsilon}{4} + \frac{\epsilon}{2} + \sum_{j \in \mathcal{F}} |Q^\pi(s, a) - Q^\pi(s, c_j)| e^{-\beta\mu} \\
 \leq & \frac{\epsilon}{4} + \frac{\epsilon}{2} + 2N \sup_a |Q^\pi(s, a)| e^{-\beta\mu}
 \end{aligned}$$

In order to have  $2N \sup_a |Q^\pi(s, a)| e^{-\beta\mu} \leq \frac{\epsilon}{4}$ , it suffices to have  $\beta \geq \frac{-1}{\mu} \log\left(\frac{\epsilon}{8N \sup_a |Q^\pi(s, a)|}\right) := \beta_0$ . To conclude the proof:

$$|Q^\pi(s, a) - \widehat{Q}_\beta(s, a; \theta)| \leq \epsilon \quad \forall \beta \geq \beta_0.$$

For a similar proof, see (Benaim, 1994). □

## 8.2. Hyper-parameter Tuning

### 8.2.1. COMMON HYPER-PARAMETERS

For all value-function-based baselines, per one episode, we performed 100 updates to their value network. For DDPG, we performed 100 updates to the value network, and 100 updates to the policy network. For TD3, we performed 50 updates to the policy due to its delayed policy updates. The target network parameters were updated in all baselines using a step size  $\alpha_{\theta^-} = 0.005$ . The maximum length of the replay buffer was fixed to 500000. Rewards were always clipped to the range  $[-20, 20]$ . We used a batch size 256. In terms of network topology, we tuned the number of nodes per layer and the number of hidden layers of each network, and chose the one that performed robustly across all 9 domains. Specifically we tried 1, 2, and 3 hidden layers each having 128 or 512 nodes. For DDPG, TD3, and input-convex neural nets, we also tried network topology parameters according to the settings suggested in the original papers.

To determine the best hyper-parameters, we ran each algorithm for 3 independent runs using the chosen hyper-parameter setting, and selected the one that performed best on average. Best performance was defined as the highest sum of rewards across the episode once training was over.

We now move to domain-dependent hyper-parameters.

### 8.2.2. RBF-DQN

For each domain, we tuned the smoothing parameter  $\beta$  using random search (Goodfellow et al., 2016) from the range  $[0.1, 3]$ . We also tuned the learning rate for RMSProp using random search from the range  $[5 \times 10^{-6}, 5 \times 10^{-2}]$ . Other hyper-parameters were kept constant across domains.

### 8.2.3. FEED-FORWARD NETWORK

For each domain, we tuned the learning rate for RMSProp using random search from the range  $[5 \times 10^{-6}, 5 \times 10^{-2}]$ . We also tuned the parameters of gradient ascent optimizer for solving  $\max_{a \in \mathcal{A}} \widehat{Q}(s, a; \theta)$ . In particular, there were two parameters, namely a step size that was tuned using random search from the range  $[0.0001, 0.1]$ , and the number of gradient ascent steps which was tuned using grid search from  $\{10, 20, 50\}$ . Other hyper-parameters were kept constant across domains.

### 8.2.4. WIRE FITTING

For each domain, we tuned the learning rate for RMSProp using random search from the range  $[5 \times 10^{-6}, 5 \times 10^{-2}]$ . All other hyper-parameters were kept constant across different domains.

### 8.2.5. INPUT-CONVEX NEURAL NETWORK

For each domain, we tuned the learning rate for RMSProp using random search from the range  $[5 \times 10^{-6}, 5 \times 10^{-2}]$ . All other hyper-parameters were kept constant across different domains.

### 8.2.6. DDPG

For each domain, we tuned the two learning rates from the range  $[5 \times 10^{-6}, 5 \times 10^{-2}]$ . Note that the learning rates for the value network and the policy network were tuned separately. For each individual domain, we tried two optimizers, namely RMSProp and Adam (Kingma & Ba, 2014). All other hyper-parameters were kept constant across different domains.

### 8.2.7. TD3

Similar to DDPG, we tuned the two learning rates for the value network and the policy network using the same range. We again tried two optimizers, namely RMSProp and Adam (Kingma & Ba, 2014). Fujimoto et al. (2018) also introduced a  $\sigma$  parameter for target policy regularization in TD3. We tuned this hyper-parameter for each domain as well using grid search and from  $\{0.01, 0.05, 0.1, 0.2\}$ . All other hyper-parameters were kept constant across different domains.

8.3. A Comparison based on Final Performance

	<b>RBF-DQN</b>	<b>DDPG</b>	<b>TD3</b>	<b>Wire Fitting</b>	<b>Feed-forward network</b>	<b>Input-convex network</b>
<b>Pendulum-v0</b>	<b>-153±28</b>	<b>-171±25</b>	<b>-160±29</b>	-821±203	-242±65	-275±48
<b>LunarLander Continuous-v2</b>	227±7	-76±118	<b>218±10</b>	-564±173	170±11	-14±54
<b>Bipedal Walker-v2</b>	<b>265±26</b>	<b>270±28</b>	177±42	-101±3	-24±1	-62±12
<b>Ant-v1</b>	<b>2766±179</b>	<b>2578±168</b>	<b>2816±83</b>	-137±105	22±4	564±151
<b>Half Cheetah-v1</b>	<b>7593±301</b>	5570±979	5853±560	-502±55	5332±63	5448±643
<b>Hopper-v1</b>	<b>3083±39</b>	877±202	578±178	11±5	1957±294	535±73
<b>InvertedDouble Pendulum-v1</b>	8020±692	7832±1221	7819±859	5905±198	448±99	<b>9346±5</b>
<b>Inverted Pendulum-v1</b>	<b>1000±0</b>	<b>1000±0</b>	<b>1000±0</b>	7±2	301±89	902±92
<b>Reacher-v1</b>	<b>-5±1</b>	<b>-5±1</b>	<b>-5±1</b>	-67±5	-17±2	<b>-5±1</b>

Figure 6. A comparison between RBF-DQN and different deep-RL baselines based on final performance.